# FEM Aided Design of Permanently Split Capacitor Motor under Different Operating Regimes

(Full text in English)

Vasilija SARAC[1]
[1]University „Goce Delcev", Faculty of Electrical Engineering, Macedonia

**Abstract**
This paper proposes a methodology for numerical modelling of permanently split capacitor motor under different operating regimes with the aid of Finite Element Method (FEM). Firstly, based on the double-field revolving theory and the method of symmetrical components, all important motor parameters and characteristics are calculated. They serve as input data in FEM based model together with the exact motor geometry and the properties of all materials. The accuracy of the calculated parameters and characteristics is verified by experiments. FEM model evaluates the electro-magnetic quantities of the motor such as the magnetic flux density in motor cross-section and the magnetic field strength, often difficult to be calculated by analytical methods. The following results are obtained - the magnetic flux density in motor cross-section and the air gap under different operating regimes such as no-load, rated load and locked rotor. They are calculated for magneto-static case i.e. frequency of 0 Hz as well as for time-harmonic case i.e. frequency of 50 Hz. The obtained results enable parts of the motor construction with high flux density to be discovered and further improved by using high quality magnetic materials.
**Keywords**: permanently split capacitor motor, method of symmetrical components, finite element method, magnetic flux density

*Received:* December, 08, 2015

## 1. Introduction

The Permanently Split Capacitor (PSC) motor is one of the mostly used single-phase motors. Most of the single-phase motors utilize auxiliary (start) winding on stator side in order to produce a starting torque and this winding is usually disconnected after motor starting. The PSC motor has neither a starting switch, nor a capacitor that are used just for starting. Instead, it has a run-type capacitor, permanently connected, in series, to the start winding. It transforms the start winding to auxiliary winding once the motor reaches the running speed (Figure 1).

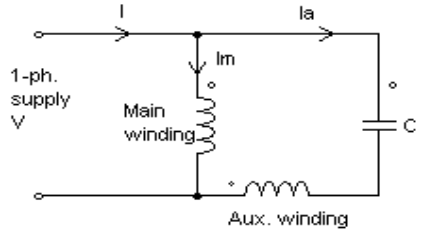


**Figure 1.** PSC motor-winding connection

Because the run capacitor must be designed for continuous use, it cannot provide the starting boost of a starting capacitor. Typically, starting torques of PCS motors are low, from 30 to 150 % of rated load, therefore these motors are not used for hard-to-start applications. However, unlike split phase motors, PCS motors have low starting currents, usually less than 200 % of the rated load current, making them excellent for applications with high cycle rates. The breakdown torque varies depending on the design type and application, through it is typically lower in comparison to the capacitor start motor. PSC motors have several advantages. They do not need to start the mechanism and can be reversed easily. In this paper, PSC motor type FMR 35/6 (Figure 2), product of the company "MicronTech" is investigated.

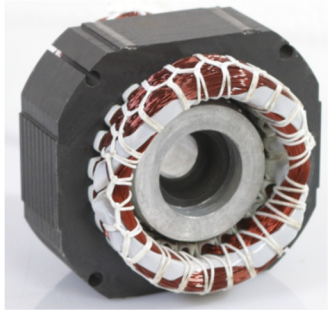

**Figure 2.** Motor layout

The motor has the following rated data: rated voltage $U_n$= 220-240 V, rated power $P_n$=124W, rated speed $n_n$=2880 rpm, rated current $I_{mn}$=1,3 A, permanent capacitor C=6μF.

The calculation of parameters and characteristics of the single-phase motors is always a challenging task since there is not always a standardized methodology for their calculation.

The complexity of the analysis of electro-magnetic phenomena inside the single-phase machine is a result of the existence of two electromagnetically coupled stator windings that produce an elliptic electromagnetic field in the motor air gap. The calculation of motor parameters and the analysis of motor performance characteristics for different operating regimes,

meaning slip-s within range (0÷1), is based on the double –field revolving theory [1]-[8]. The calculated parameters are input data for the motor numerical model that uses FEM for calculation of the magnetic flux density distribution in motor cross-section under different operating regimes (no-load, rated load and locked rotor). The numerical model is designed, based on the motor exact geometry and the properties of all materials. Maxwell set of equations, which define the magnetic vector potential **A** and the magnetic flux density **B**, are solved for two different cases: magneto-static (frequency f=0 Hz) and magneto-dynamic (frequency f=50 Hz). The complete distribution of the magnetic flux density in motor cross-section enables parts of motor construction with high flux density to be discovered, which contributes to the further improvement of motor construction [9].

## 2. Analytical calculation of parameters and characteristics

The development of the mathematical model of single-phase motor is based on the double-field revolving theory. The method of symmetrical components is used as a mathematical toll and consequently the unsymmetrical currents and voltages of the two stator windings of PSC motor, denoted as general vector **A** (Figure 3), may be decomposed into two symmetrical systems consisted of the forward and backward or direct and inverse components of the symmetrical systems [3].

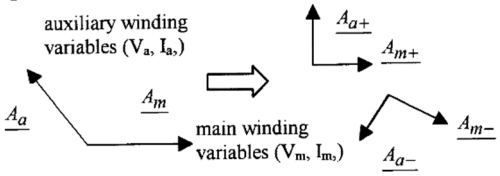


**Figure 3.** Symmetrical components of two-phase system

The method of symmetrical components is used for motor performance characteristic calculation and the first step in their calculation is to determine all motor parameters: $R_{sm}$-main stator winding resistance, $X_{sm}$-main winding leakage reactance, $R_{sa}$-auxiliary stator winding resistance, $X_{sa}$-auxiliary stator winding leakage reactance, $X_{mm}$-magnetizing reactance, $R_{rm}$-rotor winding resistance, $X_{rm}$-rotor winding leakage reactance.

Their values are presented in Table 1.

**Table 1.** Motor parameters

| Parameter | Value |
|---|---|
| $R_{sm}$ [Ω] | 13.57 |
| $X_{sm}$ [Ω] | 31.71 |
| $R_{sa}$ [Ω] | 75.6 |
| $X_{sa}$ [Ω] | 53.51 |
| $X_{mm}$ [Ω] | 425.96 |
| $R_{rm}$ [Ω] | 10.505 |
| $X_{rm}$ [Ω] | 20.5 |

The calculation of motor parameters is based on the motor manufacturer data regarding the motor stator and rotor dimensions, the number of slots and the length of motor air gap. The main stator winding is placed in sixteen stator slots distributed under one pair of poles. The auxiliary winding is placed in the smaller stator slots and occupies eight slots altogether. The rotor winding is constructed as squirrel cage with rotor bars distributed in the rotor slots and short-circuited by end rings.

After calculation of the rotor parameters, the direct and inverse impedances of the main stator winding $\underline{Z_{m+}}$ and $\underline{Z_{m-}}$ are determined as well as the mutual impedance between the main and auxiliary winding $\underline{Z_a^m}$ and consequently they are used for calculation of the direct and inverse components of the current in the main stator winding $\underline{I_{m+}}$ and $\underline{I_{m-}}$ [3]. The direct and inverse components of the rotor winding impedance $\underline{Z_{r+}}$ and $\underline{Z_{r-}}$ are calculated as well [6]. They are used for calculation of the direct and inverse components of the rotor currents $\underline{I_{r+}}$ and $\underline{I_{r-}}$. The supply current is calculated from:

$$I_s = \left| \underline{I_{m+}} + \underline{I_{m-}} + j\frac{\underline{I_{m+}} - \underline{I_{m-}}}{a} \right| \quad (1)$$

The currents in the main stator winding, the auxiliary winding and the rotor winding are calculated respectively:

$$I_m = \left| \underline{I_{m+}} + \underline{I_{m-}} \right| \quad (2)$$

$$I_a = \left| j\frac{\underline{I_{m+}} - \underline{I_{m-}}}{a} \right| \quad (3)$$

$$I_r = \left| \underline{I_{r+}} + \underline{I_{r-}} \right| \quad (4)$$

where $a$ - represents the ratio of turns of the auxiliary stator winding- $N_a$ and the main winding- $N_m$. Direct and inverse components of electromagnetic torque are found from [3]:

$$T_{e+} = \frac{2p}{\omega_1} I_{m+}^2 \left[ \mathrm{Re}\left(\underline{Z_+}\right) - R_{sm} \right] \quad (5)$$

$$T_{e-} = -\frac{2p}{\omega_1} I_{m-}^2 \left[ \mathrm{Re}\left(\underline{Z_-}\right) - R_{sm} \right] \quad (6)$$

Where p is the number of pair of poles and $\omega_1$ is the angular frequency [rad/s]. $Z_+$ and $Z_-$ are direct and inverse impedances obtained from main and rotor winding parameters as well as from magnetizing reactance.

Electromagnetic torque is obtained from:

$$T_e = T_{e+} + T_{e-} \quad (7)$$

The input power is calculated from:

$$P_1 = V_s |I_s| \cos\varphi \tag{8}$$

$V_s$ is the motor supply voltage, $I_s$ is the supply current and cosφ is the power factor.

The power factor is calculated from:

$$\cos\varphi = \frac{real(I_s)}{I_s} \tag{9}$$

The efficiency factor is calculated from input power-$P_1$ and output power $P_2$ of the motor:

$$\eta = \frac{P_2}{P_1} \tag{10}$$

The obtained values of the motor characteristics at rated load operating regime are compared with the data from experiment for the purpose of verification of the proposed methodology and they are presented in Table 2.

**Table 2.** Comparison between calculated and measured data

| **Rated operation, s=0.04** | | |
|---|---|---|
| **Parameter** | **Math. model** | **Experiment** |
| Rated torque [Nm] | 0.412 | 0.402 |
| Rated supply current [A] | 1.6 | 1.32 |
| Maximum output power [W] | 215 | 210 |
| Maximal torque [Nm] | 0.766 | 0.80 |
| **Start-up, s=1** | | |
| Starting torque [Nm] | 0.1 | 0.13 |
| Starting supply current [A] | 3.5 | 4 |

The presented results in Table 2 have proved that the proposed methodology for the calculation parameters and characteristics of the motor is accurate enough, therefore the analysis is extended for different operating regimes and different motor slips. The validation of the proposed analytical motor model is important for further motor analysis and development of the motor numerical FEM model, since parameters and characteristics of the motor such us currents in all motor windings are input data in this model and consequently contribute to accurate determination of magnetic field density in the motor air gap and the cross-section.

The motor performance characteristics are calculated for the complete range of motor operating regime, i.e. slip-s within range 0÷1, and they are presented in Figures 4-6, for the motor output torque-T, the efficiency factor-η, the power factor-cosφ, the input and output power-$P_1$ and $P_2$, and the currents in all three windings: $I_s$, $I_m$ and $I_a$ respectively.

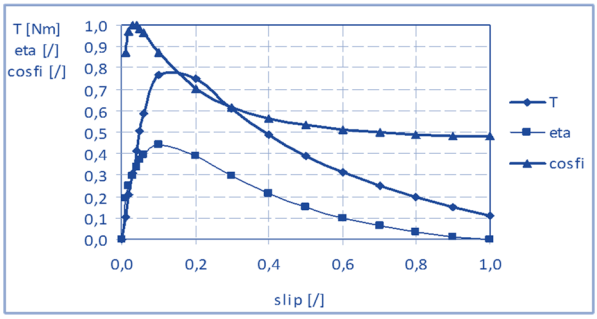


**Figure 4.** Torque, efficiency and power factor for different slips

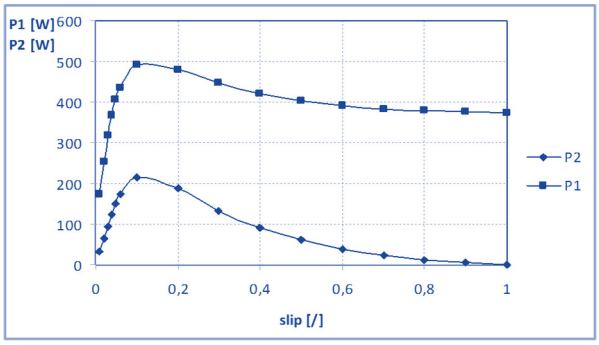


**Figure 5.** Input and output power for different slips

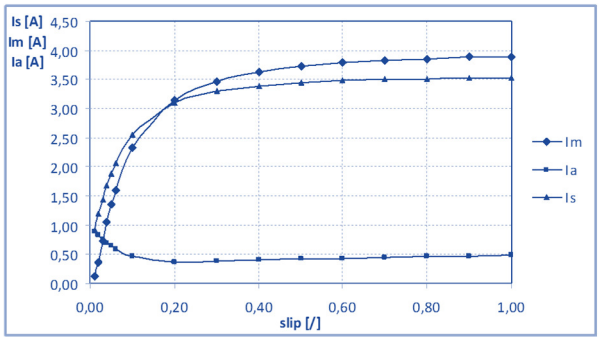


**Figure 6.** Motor currents for different slips

## 3. FEM model of the motor

### *3.1. Problem definition*

Throughout the recent years, FEM has proved itself as valuable tool in electric machine analysis when calculating parameters and characteristics of the variety of electromagnetic devices [10]-[18]. The analysis of the electromagnetic phenomena inside single-phase machines is always a challenging task due to the existence of the two stator-windings mutually electro-magnetically coupled, which together with the rotor winding produce an elliptic electromagnetic field in the motor air gap. Therefore, a special attention is paid on the proper motor modelling regarding distribution of currents in motor FEM model, by taking into account the current in the main and the auxiliary stator winding and their phase displacement due to the presence of capacitance in the auxiliary stator winding [19]-[26]. The original motor models have been developed, which are

suitable for FEM analysis based on the previously calculated motor parameters and characteristics. Another important issue is the proper modelling of different operating regimes such us: no-load, rated load or locked rotor. Therefore, the rotor bars conductivity is adjusted to the motor slips correspondingly, i.e. the motor operating regimes as well as the adequate values of motor currents and parameters are input in the motor models. Two different approaches are used for analysing electromagnetic phenomena inside the motor: magneto-static and time-harmonic. Consequently, two different FEM motor models are constructed. For magneto-static case, the currents in all motor windings are input since electromagnetic field is time invariant at frequency f=0 Hz so the rotor current cannot be freely induced. For time-harmonic case, the second motor model is developed, in which the currents are input only in the stator windings while in the rotor winding, the current is freely induced at frequency f=50 Hz due to the specific motor modelling. Properties of all materials inside the motor are defined as well. A very important issue is to define the boundary conditions on the motor outer geometry. In this case, Dirichlet-boundary conditions are used. Another important subject in the motor modelling is defining the mesh of finite elements. By dividing the motor's cross section into large number of regions, i.e. elements with simple geometry (triangles), the true solution of magnetic vector potential **A** is approximated by a very simple function. In magneto-static approach, all electromagnetic quantities are time constant and they are analysed in certain moment of time, i.e. at frequency f=0 Hz, while in time-harmonic magnetic approach, they are analysed at frequency f=50 Hz. In time-harmonic motor model, only the currents in stator windings are input while in the rotor winding, the current is freely induced. On that way, the analysis of electromagnetic phenomena inside the motor is closer to the real electromagnetic processes inside the machine when it is supplied with voltage 220 V, 50 Hz. FEM analysis of the motor is divided into three parts: pre-processing, processing and post-processing part. In the pre-processing part, the motor geometry is defined and the material properties as well. The calculation of current densities is performed, the boundary conditions on outer motor geometry are defined, and the finite element mesh is defined as well. In order to execute the processing part and to obtain output results, the system of Maxwell's equations should be solved. They differ in both cases: magneto-static and time-harmonic. Magneto-static problems are problems in which the fields are time-invariant. In this case, the field density **H** and the flux density **B** must obey:

$$\nabla x\mathbf{H} = \mathbf{J} \tag{11}$$

$$\nabla x\mathbf{B} = 0 \tag{12}$$

and they are subject to a constitute relation between **B** and **H** for each material:

$$\mathbf{B} = \mu\mathbf{H} \tag{13}$$

For the magneto-static problem and the non-linear B-H relation FEM solves the equation [27]:

$$\nabla x\left(\frac{1}{\mu(\mathbf{B})}\nabla x\mathbf{A}\right) = J \tag{14}$$

The advantage of using the vector-potential formulation is that all the conditions to be satisfied are combined into a single equation. If **A** is found, **B** and **H** can be deduced by differentiation of **A**. The properties of all materials are input in motor model.

Besides inputting the magnetization curve as B=f(H) (Figure 7), the lamination of magnet material according to Figure 8 (a) and the fill factor are input as well. The result of this model is that the laminations with hysteresis and the eddy currents are taken into account.

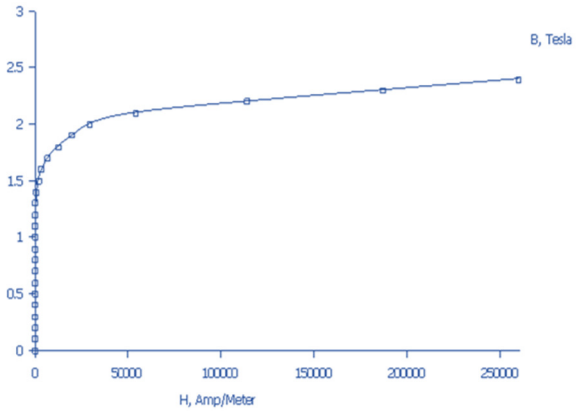


**Figure 7.** Magnetization characteristic B=f(H)

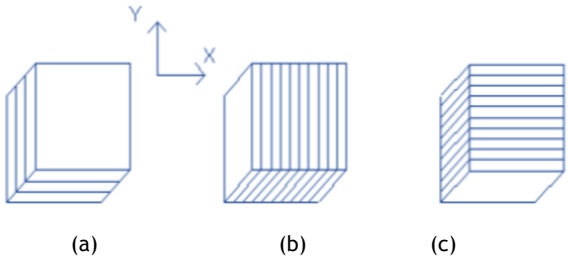


**Figure 8.** Possible core laminations in motor design

In order to determine the magnetic vector potential **A,** it is necessary for the whole domain i.e. motor's cross-section to be divided into numerous elements. The finite element mesh consisted of N=49686 nodes and 98954 elements is created at cross-section of PSC motor (Figure 9).

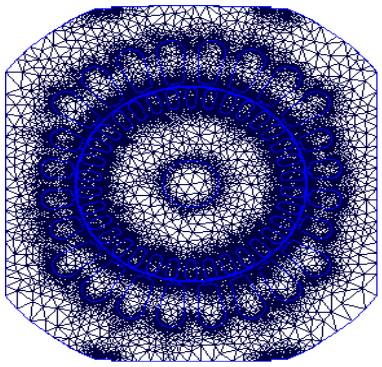

**Figure 9.** Finite element mesh at motor cross-section

For magneto-static case, it is necessary to input the current densities in all three motor windings as well as the properties of the materials for all windings. Having all three currents in the motor model, the program is run at stator frequency f=0 Hz.

When analysing induction machines, considering their AC excitation, the air gap magnetic field is always a time-varying quantity. In the materials with non-zero conductivity, the eddy currents are induced, consequently the field problem turns into magneto-dynamic i.e. non-linear time-harmonic problem. When the rotor is moving, the rotor quantities oscillate at slip frequency. In this case, the rotor bars conductivity σ is adjusted corresponding to the slip. Consequently, the following equation is going to be solved numerically [27]:

$$\nabla x\left(\frac{1}{\mu(\mathbf{B})}\nabla x\mathbf{A}\right)=-\sigma\dot{\mathbf{A}}+\mathbf{J}_{src}-\sigma\nabla V \tag{15}$$

where $\mathbf{J}_{src}$ represents the applied current sources. The additional voltage gradient ∇V in 2-D field problems is constant over the conduction body. Strictly speaking, the permeability μ should be constant for harmonic problems. However, FEM retains a nonlinear relationship in the harmonic formulation, allowing the program to approximate the effects of saturation on the phase and amplitude of the field distribution. FEM also takes the inclusion of complex and frequency-dependent permeability in time-harmonics problems into consideration. These features allow the program to model the materials with thin laminations and to model the hysteresis effects approximately.

For time-harmonic case, the program is run at constant frequency f=50 Hz. In the motor model, only the currents in the stator windings are input, while the current in the rotor winding is freely induced.

### *3.2. Post processing and output results*

Both programs with motor models are run and post processing results such as the magnetic flux density distribution in motor's cross section as well as the distribution of magnetic flux density in the middle of the air gap are obtained.

Figures 10, 11 and 12 present the magnetic flux density distribution in motor cross-section at no-load, rated load and locked rotor respectively.

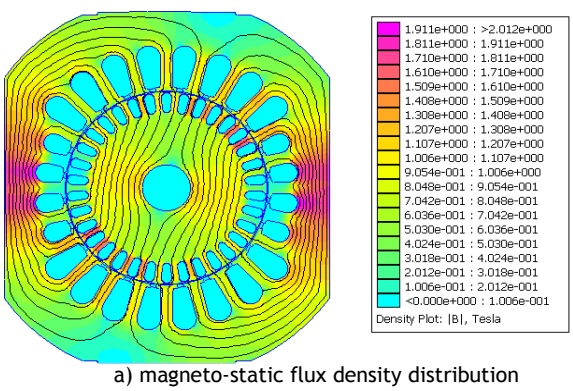


a) magneto-static flux density distribution

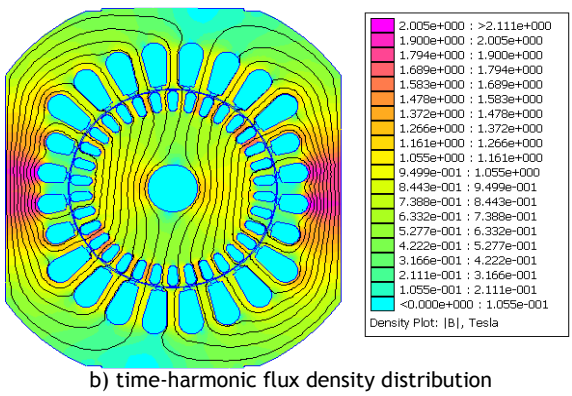


b) time-harmonic flux density distribution

**Figure 10.** Flux density distribution at no-load

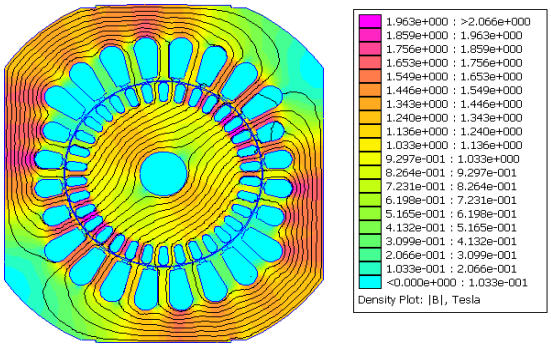


a) magneto-static flux density distribution

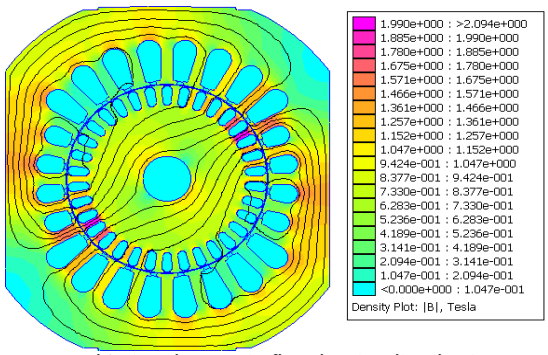


b) time-harmonic flux density distribution

**Figure 11.** Flux density distribution at rated load

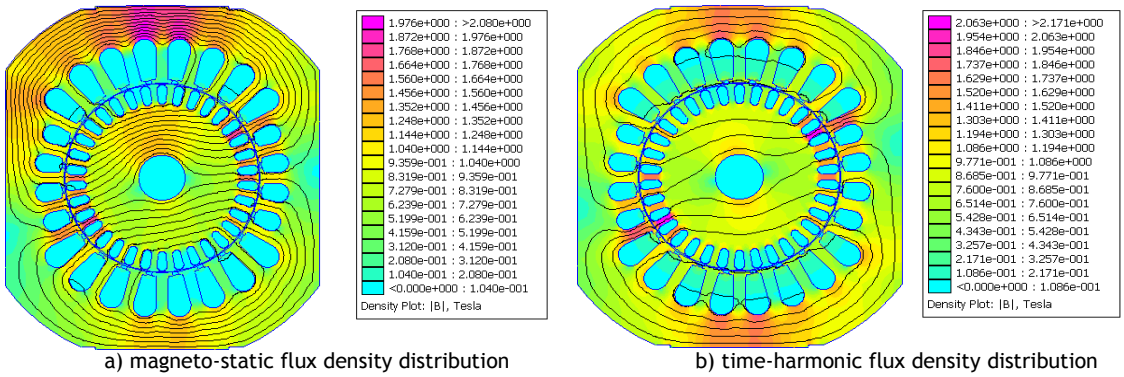


a) magneto-static flux density distribution b) time-harmonic flux density distribution

**Figure 12.** Flux density distribution at locked rotor

From the presented results, some increase of the magnetic flux density at locked rotor operation compared to rated load and no-load operating regime is evident, due to the increased currents in all three windings. The magnetic flux density in motor air gap per pole is plotted for rated operation regime as it is presented in Figure 13.

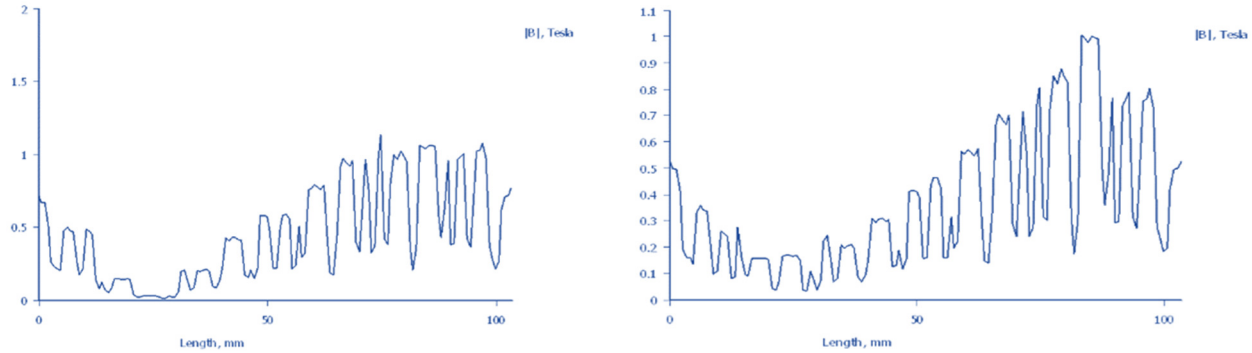


a) magneto-static case b) time-harmonic case

**Figure 13.** Flux density distribution in air gap at rated load

In Figures 14 and 15, the magnetic flux density distribution in motor air gap for no-load and the locked rotor operation are presented.

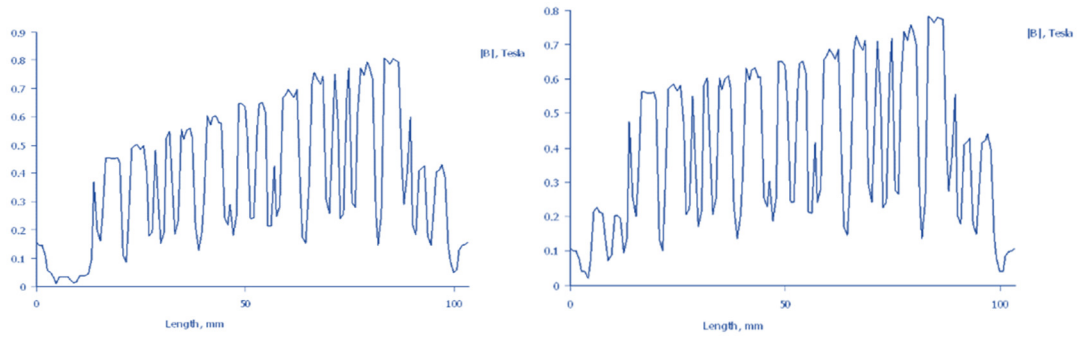


a) magneto-static case b) time-harmonic case

**Figure 14.** Flux density distribution in air gap at no-load

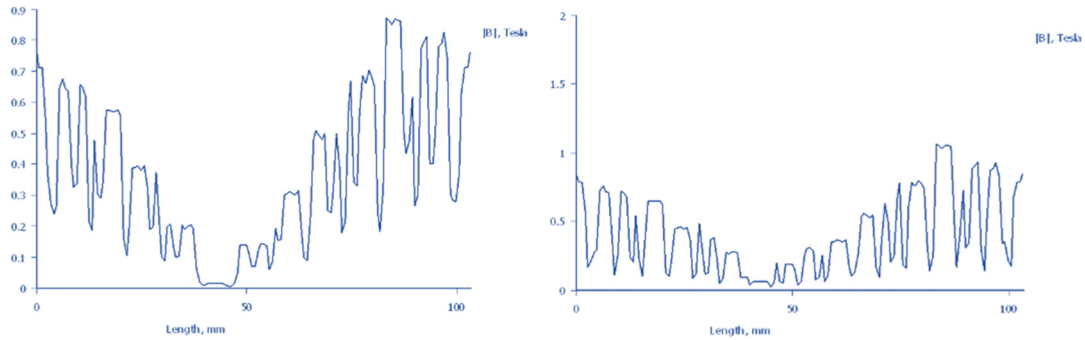


a) magneto-static case b) time-harmonic case

**Figure 15.** Flux density distribution in air gap at locked rotor

From presented results in Figures 13, 14 and 15, it is evident that value of magnetic flux density in motor air gap for magneto-static and time-harmonic case has similar values. This can be expected taking into consideration that same operating regime of the motor is evaluated. In time harmonic case currents is rotor cage winding are freely induced while in magneto-static case all the currents are input in motor model. Similarity of the results confirms the accuracy of the proposed models in both cases.

In FEM model, the electromagnetic torque-$T_e$ is calculated from Maxwell-Stress tensor. The results are read out in the motor air-gap using the time-harmonic motor model. The obtained results of the electromagnetic torque are compared with the ones from the analytical calculation showing reasonable similarity and confirming the accuracy of the proposed analytical and numerical model of the motor (Figure 16).

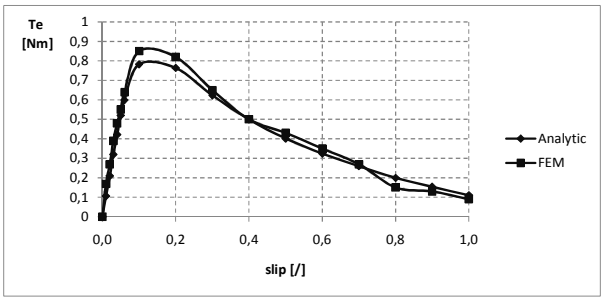


**Figure 16.** Comparison of torque from mathematical and FEM model

The values of the magnetic flux density in the motor air-gap obtained by FEM calculation are confirming the predicted average value of the magnetic flux density of 0.7 T in the analytical model used for the calculation of parameters and characteristics. The obtained values of the magnetic flux density and its distribution in motor cross-section in magneto-static and time-harmonic case are close to one another. Taking into consideration that two different methods are involved for the calculation of the magnetic flux density and two different FEM motor models as well, the similarity of the obtained results confirms the accuracy of the analytical motor model. This model also contributes to the input parameters of FEM model and to the accuracy of two different numerical motor models developed in FEM. In some points of the motor cross-section (rotor teeth), high values of the magnetic flux density are evident, which can cause saturation of the magnetic core. It is desirable the high quality magnetic materials to be implemented in the motor construction, in order to avoid high values of magnetic flux density, core saturation and high values of iron losses. In general, the implementation of certain type of materials in machine constructions is a compromise between costs and motor performance.

## 4. Conclusions

Analysis of small single-phase micro motors is always a challenging task due to complexity of electromagnetic processes inside this type of the machines and the existence of two stator windings electromagnetically coupled one to another producing elliptic electromagnetic field in the air gap of the motor. Double field revolving theory and method of symmetrical components is used for obtaining motor mathematical model and calculation of parameters and steady-state performance characteristics. Motor performance characteristics are calculated for different motor operating regimes i.e. motor slips. Developed mathematical model of the motor is verified by comparison of calculated motor characteristics with the ones obtained from the producer. Some electromagnetic parameters such as magnetic flux density in the air gap and cross-section of the motor are difficult to be predicted or calculated by analytical methods. Therefore, numerical model of the motor is constructed based on Finite Element Method that uses as input parameters calculated currents in all motor windings based on method of symmetrical components. Two different approaches are applied in calculation of magnetic flux-density in motor cross-section: magneto-static at frequency 0 Hz and time-harmonic approach at frequency 50 Hz. In magneto-static case, the magnetic flux density distribution in certain moment of time is calculated. Consequently, currents are input in all motor windings in order magnetic flux density in motor-cross section to be plotted. In time harmonic approach currents are input only in stator windings while in the rotor winding it is freely induced. Both approaches show similar results regarding maximal value of magnetic flux density in motor cross-section and its distribution. In some rotor teeth, it is noticeable higher value of magnetic flux density near to the point of saturation, which can be lowered by using high quality magnetic materials. Proposed motor numerical model is highly dependent on accurate calculation of motor parameters: resistances and reactances. The latter ones are calculated using analytical formulas that give only approximate values of the reactances. Approach that is more accurate is the numerical one, which should be used for calculation of reactances. This will be the further focus of author's research.

## 5. References

[1] W.H. Yeadon, A.W.Yeadon, Handbook of small electric motors, McGraww-Hill, (2003) pp. 6.61~6.69.

[2] M. Popescu, T. J. Miller, M. McGilp, G. Strappazzon, N. Traivillin and R. Santarossa, "Asynchronous Performance Analysis of a Single-Phase Capacitor-Start, Capacitor-Run Permanent Magnet Motor," *IEEE Trans. on Energy Conversion*. 2005; Vol.20, (no.1):

pp.142-150.
[3] I. Boldea, S.A.Nasar, "The Induction Machines Design Handbook", CRC Press, (2010) pp. 791~805.
[4] V.K.Ghail, L.M. Saini, J.S.Saini, "Paramter Estimation of Permanent-Split Capacitor Run Single-Phase Induction Motor Using Computed Complex Volage Ratio", *IEEE Transaction on Industrial Electronics*, 2014, vol.61 (no.2): pp. 682-692.
[5] G.Madescu, M.Greconici, M.Biriescu, M.Mot, "Two-phase capacitor motor analysis in steady-state symmetrical conditions" *, in Proc. of International Conference on Optimization of Electrical and Electronic Equipment ,* Bran, pp. 375-380, 2014.
[6] I.E.Davidson, "Performance Calculation of a Shaded-Pole single Sided Linear Induction Motor Using Symmetrical Components and Finite Element Method" *Journal Electromotion* 1997; vol. 4, (no.4): pp. 139-145
[7] T. A. Lettenmaier, D.W. Novotny, and T. A. Lipo, "Single-phase induction motor with an electronically controlled capacitor," *IEEE Transactions on Industrial Application*. 1995; vol. 27 (no. 1) pp. 38–43.
[8] S. Williamson, A. C. Smith, "A unified approach to the analysis of single phase induction motors," *IEEE Transactions on Industry Application*. 1999; vol.35, (no.4): pp. 837–843.
[9] J.Chvdivani, V.Kujan, M.Perny, L.Huttner, R.Eric, V.Saly, "Issues of Electromagnetic design of Synchronous Brushless Motors with Concetrated Winding", *Electrical Engineering, Electronic, Automation*, 2014, vol.62 (no.2): pp.24-29.
[10] Z. Ferkova, "Comparison between 2D and 3D Modeling of induction machine using Finite Element Method ", *Power Engineering and Electrical Engineering*, 2015, vol.13 (no.2): pp.120-126
[11] D. Olaru, "Field analysis in the structure of dual gap electromagnetic actuators", *Electrical Engineering, Electronic, Automation*, 2012, vol.60 (no.1): pp.40-43.
[12] M.Modreanu, M-l. Andrei, "numerical Modeling of Two-Chanel Limited Angle Torque Motor", *Electrical Engineering, Electronic, Automation*, 2014, vol.62 (no.1): pp.26-31.
[13] I.Yatchev, M. Rudnicki, K. Hinov, V. Gueorgiev, "Optimization of permanent magnet needle actuator", *COMPEL*, 2012, vol.32 (no.3): pp.1018-1028.
[14] E.Huner, M.C. Akuner, U. Demir, "A new approach in application and design of toroial axial-flux permanet magnet open-slotted NN type (TAFPMOS-NN) motor", Technical Gazette, 2015, vol.22 (no.5), pp. 1193-1198.
[15] V.Sarac, T.Atanasova-Pacemska, D.Minovski, G. Cogelja, M.Smitkova, C.Schulze, "Optimized and numerical models of electromechanical devices coupled with computation of performance characteristics", *Journal of Electrical Engineering*, 2015, vol .66 (no.1): pp.39-45.
[16] T.Vaimann, A.Belachen, A.Kallase, "Changing the Magnetic Flux Density Distribution in a Squirrel-Cage Induction Motor with Broken Bars", *Elektronika ir Elektrotechnika*,2014, vol.20, no.7, pp.11-14.
[17] P.Paplicki, "Optimization of Electrically Controlled Permanent Magnet Synchonous Machine to Improve Flux Control Range " *Elektronika ir Elektrotechnika*, 2014, vol.20, no.10, pp.17-22.
[18] S.Masic, J.Corda, S.Smaka, "Computation of Static, Steady-state and Dynamic Characterisitcs of the Switched Reluctance Motor", *Automatika*,2002, vol.43 (no3-4), pp. 109-117.
[19] L.Petkovska, G.Cvetkovski, "FEM based assessment of capacitor sizing characteristics of a single-phase induction motor," *Prezglad Elektrotechniczny*. 2010; vol.86 (no.12): pp. 113-116.
[20] R.Campenau, M.Cernat, "Two Speed Single Phase Induction motor with Electronically Controled Capacitance", *Advances in Electrical and Computer Engineering*, 2014, vol.14 (no.3): pp.137-140.
[21] A.Negoita, G.Scutaru, I.Peter, "Numerical modeling and experimental analysis of the magnetic noise of the single-phase inverter-fed permanent split-capacitor motor", *in Proc. of 13th International Conference on Optimization of Electrical and Electronic Equipment* , Brasov, pp. 600-605, 2012.
[22] T. Tudorache, L. Melcescu, "FEM optimal Design of Energy Efficient Induction Machines", *Advances in Electrical and Computer Engineering*, 2009, vol.9 (no.2): pp.137-140.
[23] V. Hrabocova, P. Rafajdus, "Radial Magnetic Forces on Single Phase Permanent Split-Capacitor Motor", *Journal of Electircal Engineering*. 2006, Vol. 57 (no.5): pp. 185-192.
[24] Y.Sun, D.Y.Lee, "Numerical Analysis of Single Phase Induction Motors by using Circuit Equations Coupled with Magnetic Field Distribution," *Journal of Magnetic*, 2013; vol.18 (no.3): pp. 255-259.
[25] K.Makowski, M.J.Wilk, "Experimental verification of field-circuit model of a single-phase capacitor induction motor", *Prezglad Electrotechniczny*. 2012; vol.88 (no.7b): pp. 116-118.
[26] D.Zhou, C.B. Rajanathan, A.T. Sapeluk, C.S. Ozveren, "Finite –Element-Aided Design Optimization of a Shaded Pole Induction Motor for Maximum Starting torque" *IEEE Transactions on Magnetics*, 2000. vol.36. pp. 3551-3554, 2000.
[27] D. Meeker, Finite Element Method Magnetics-Version 4.2, User's Manual.

## 6. Biography

**Vasilija SARAC** was born in Skopje (Macedonia), on July 5, 1972.
She graduated the Faculty of Electrical Engineering in Skopje (Macedonia), in 1995.
She received the PhD degree in electrical engineering from the Faculty of Electrical Engineering (Macedonia), in 2005.
She is Professor at the University Goce Delcev, in Stip (Macedonia).
Her research interests concern: electric machines and power electronics.
*Correspondence address*: University „Goce Delcev", Faculty of Electrical Engineering, P.O. Box 201, 2000 Stip, Macedonia, e-mail: vasilija.sarac@ugd.edu.mk